Chapter 2
Ion Transport and Focal Properties of an Ellipsoidal Electrode Operated at Atmospheric Pressure

2.1 Introduction

Most frequently, ions are transported from ambient pressure and manipulated under low pressure conditions. While a vacuum environment is necessary to make precise measurements of an ion's mass-to charge ratio, the ability to effectively control ion trajectories and spatially manipulate ions without the use of vacuum systems is of great interest in a number of different fields. Modifications to surfaces made using low energy molecular ion beams [1–9] are of particular note. Such modifications include cases in which the ion/surface interaction occurs at atmospheric pressure [10, 11]. Applications include the chemical functionalization (derivatization) of surfaces [12, 13] and the preparation of thin films [14, 15]. While thin film preparation typically uses exposure to highly controlled yet poorly characterized plasmas [16], polymer film deposition using ion beam conditioning has become increasingly common [17]. Ambient ionization, particularly in the field of analytical mass spectrometry relies on the ionization and subsequent transfer of ions to a vacuum system for analysis. This field focuses on the analysis of samples via mass spectrometry in their native state, with little-to-no sample preparation. A wide variety of ambient ionization methods have been developed and include spray, laser, and plasma techniques which are used to generate representative ions [18, 19]. The growth of interest in gas-phase ion chemistry under ambient environment raises obvious concerns regarding ion transport and focusing at atmospheric pressure. An understanding of factors which contribute to the efficiency by which ions are transported has come both empirically (e.g. the transport over several meters of ions generated by desorption electrospray ionization, and their delivery to a mass analyzer [20]) as well as through fluid dynamics simulations [21]. These simulations have confirmed that once laminar flow is established in a transport tube, modest suction will move typical organic ions long distances through air without significant losses.

Z. Baird, *Manipulation and Characterization of Electrosprayed Ions Under Ambient Conditions*, Springer Theses, DOI 10.1007/978-3-319-49869-0_2

The issue of ion focusing in air is has importance beyond the ambient ionization methods. In particular, all forms of spray ionization, including electrospray ionization (ESI), yield droplets, the fission of which results in a highly dispersed spray plume in which the ion concentration decreases rapidly with distance from the source [22]. This undesirable effect is compounded by the fact that the droplets undergo further fission and desolvation before producing gas-phase ions that can be analyzed by a mass spectrometer. Increased distances of travel are needed for more effective desolvation [23, 24]. On the other hand, the small sampling orifices (generally 1 mm or less, inner diameter) needed for vacuum compatibility greatly restrict the fraction of ions that may be sampled from the spray plume. Because of these factors, ion collection efficiency is low, typically a small fraction of the ions produced (often <0.1 %) by the ionization source [22, 25].

Multipole ion guides based on collisional focusing through the application of radio frequency (RF) fields have been utilized to increase transport efficiency at lower pressures (0.1–10 mtorr) but the same effect is not observed at atmospheric pressure [26, 27]. Another popular approach is through the use of electrodynamic ion funnels. Ion funnels are composed of stacked ring electrodes of decreasing diameter to which DC and RF potentials are applied. In some cases these have improved sensitivity by more than 10 fold when operated in the first differentially pumped regions of a mass spectrometer. However, the ion funnel is only effective in the pressure range of 0.1–30 torr and is a mechanically complex device [28]. Other methods utilizing stacked ring electrodes have also been demonstrated as a means of increasing ion transmission; however their function is limited to intermediate pressures (ca. 1 mtorr—1 torr). Such methods include the traveling wave ion guide which uses electrodynamic potentials to confine ions radially along with a superimposed voltage pulse to transport ions axially, and the periodic focusing ion guide, which uses only DC potentials to provide periodic ion focusing [29, 30]. As the majority of ion loss takes place at the atmospheric pressure interface of a mass spectrometer, improvement in transport from ambient pressure to the first differentially pumped region is needed to improve sensitivity significantly.

Herein is described the use of a simple elliptical electrode to which only DC potentials are applied to facilitate the efficient transport and focusing of ions at atmospheric pressure. An ellipsoidal shape was chosen to be compatible with the intended future use of an array of spray tips as a means of increasing ion currents. The ellipsoidal shape provides symmetry in the sprayer orientation as each sprayer can be angled to spray towards the same point while experiencing equivalent potentials imposed by the focusing electrode structure. Interest is concentrated on ions produced by ion sources which have low solvent flow rates, typified by nanoESI. The focal properties of the electrode system is explored through the use of a detector that operates at ambient pressure. Quantitative measurements of ion transfer efficiency are made using ionized dyes which, after soft landing onto a surface, can be rinsed off and quantified spectrophotometrically. When interfaced to the atmospheric pressure inlet of a mass spectrometer, the ion optical system described here is shown to increase ion transport efficiency by a factor of 100 over distances of several centimeters.

2.2 Experimental

2.2.1 Chemicals and Instrumentation

All mass spectra shown herein were taken on a Thermo LTQ linear ion trap mass spectrometer (Thermo Scientific, San Jose, CA, USA) over a mass range of *m/z* 100–2000. Prior to use, the instrument was calibrated according to procedures outlined in the LTQ user manual. Solutions for positive ion calibration were prepared in-house and consisted of a mixture of caffeine, a short chain peptide salt (Met-Arg-Phe-Ala acetate, MRFA), and Ultramark 1621. For negative spectra sodium dodecyl sulfate and sodium taurocholate was included in the positive ion mixture. These solutions were prepared according to instructions provided in the user manual. Detection of the spatial distribution of ions at atmospheric pressure was accomplished through the use of an IonCCD™ detector system (OI Analytical, Pelham, AL, USA) with an integration time of 100 ms. Experiments in which the transport efficiency of ions was tested utilized a 1 mM solution of rhodamine B in 4:1 methanol:water (v:v). A Cary 300 UV–Visible spectrophotometer (Agilent Technologies, Santa Clara, CA, USA) was used for the collection of absorption spectra. Chemicals and solvents were purchased from Sigma-Aldrich (St. Louis, MO, USA).

2.2.2 Ion Transport and Beam Profiling

The assembly used to demonstrate the transmission and focusing of ions beams at atmospheric pressure in the experiments discussed within this chapter is shown in Fig. 2.1 as a cutaway view with relevant axes identified. It was manufactured from a solid stainless steel block which was milled out to form a polished, half-ellipsoidal cavity (4.3 and 1.8 cm major and minor radii, respectively). Holes were drilled on the top portion of the block, to allow for the insertion of nanoESI tips for the generation of ions, as well as a single inlet on the bottom portion through which a supplementary gas flow could be introduced. Dry nitrogen was delivered from a compressed cylinder for experiments in which a gas flow was employed. A polyether ether ketone spacer (PEEK) provided electrical isolation of the ellipsoidal electrode from grounded aluminum plate covering the opening of the cavity. For all experiments the spacing between the aluminum plate and the opening of the stainless steel electrode (z = 0) was 2 mm.

Generation, transport, and subsequent focusing of ions was accomplished by first inserting a nanoESI spray tip through one of several holes in the top of the steel electrode. Once the spray tip was inserted, the potential on the spray tip and ellipsoidal electrode were adjusted such that the difference between the two was the effective spray voltage, and the difference between the electrode and aluminum plate was the focusing potential. For example, a potential of 3 kV applied to the electrode, 4.0 kV to the sprayer, with the aluminum plate held at ground results in a

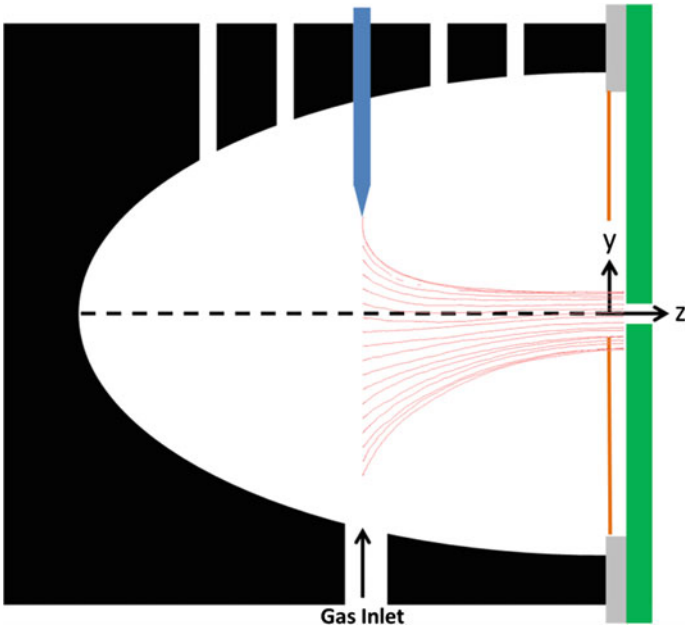

Fig. 2.1 Two dimensional representation of focusing assembly showing the stainless steel electrode (*black*), spray tip (*blue*), PEEK insulator (*gray*), and the grounded aluminum plate (*green*). Direction of axes are shown in the lower *left* with the x-axis orthogonal to the paper. The *dashed line* represents the center (z) axis of the electrode and the *orange line* is used to show the opening plane of the ellipse and is used to define z = 0. *Red traces* are plots of ion trajectories

positive-mode electrospray at a spray voltage of 1.0 kV with a focusing potential of 3.0 kV. Focusing potentials ranging from 1 to 6 kV with spray voltages in the range of 0.6–3 kV were used for all experiments described.

The full profile of the ion beam exiting the ellipse was determined by mounting the IonCCD™ with the pixel axis parallel to the y-axis and sprayer. Ion intensity profiles were taken in 0.5 mm increments across the x-axis as shown in Fig. 2.2. This experiment, including the ionization, ion transport, and detection steps was done in air without supplementary gas flow. The elliptical electrode and sprayer were held at potentials of 4 and 5 kV, respectively, while the sprayer was 25 mm from the opening plane of the ellipse (z = −25 mm). The instrument calibration mixture was used as the spray solution in all cases.

2.2.3 Ion Transport Efficiency

The efficiency of ion transport achieved with the use of the elliptical electrode assembly was explored by spraying a known amount of rhodamine B solution (1 mM)

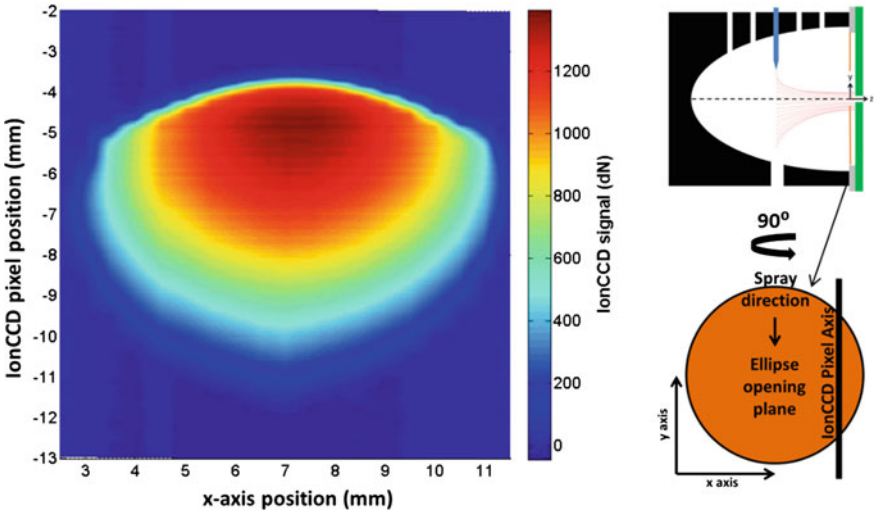

Fig. 2.2 Intensity profile of ion beam exiting ellipse in arrangement shown in Fig. 2.1, with the grounded aluminum plate replaced by an IonCCD™ detector. Potentials on ellipse and sprayer were 4 and 5 kV, respectively. Experimental setup for profiling experiment is shown in the *right* segment of figure

at different distances from the counter electrode (grounded aluminum plate) with and without the use of the elliptical electrode. The ions created were directed to and collected on the grounded aluminum plate. The material deposited on a square 1 cm^2 area corresponding to the most intense region of each deposited spot was redissolved in 1:1 methanol:water (v:v) and the solutions were analyzed for concentration by UV–Vis spectrophotometry, by employing standards of known concentration to construct a calibration curve. Quantitation was based on maximum absorbance at a wavelength of 551 nm where the molar absorptivity is 105,700 M^{-1} cm^{-1}.

2.2.4 Ion Trajectory Simulation

Several simulations were performed using the SDS algorithm to determine the trajectories of ions within the electrode and analyze the effect of varying potentials applied to each component as well as the positioning of the nanoESI tip within the electrode. The files used to generate the geometry for machining the electrode were converted to potential array (PA) files using the SL Toolkit included with SIMION 8.0. These arrays were refined using the skipped point refining method to solve for the electric field within the electrode. In each simulation the reduced mobility and diameter of each ion was estimated via the SDS algorithm. 2D images of simulated ion intensity at the deposition surface were constructed from simulation data using custom Matlab programs developed for SIMION data analysis.

2.2.5 Mass Spectrometer Interface

The electrodes were coupled to the atmospheric pressure inlet (API) of the mass spectrometer by drilling a 2.36 mm hole through the aluminum plate and inserting the 3.15 mm protrusion of the 2.28 mm outer diameter API capillary. The voltage on the capillary, as set in the LTQ software, was 15 V and electrical contact caused the potential on the aluminum plate to match this. Ions were sampled into the vacuum system of the MS through combined effects of suction at the opening of the API capillary as well as electrostatic focusing as a result of the potential applied to the focusing electrode. It is important to note that because of the relatively large area (1 cm^2) to which focused ions are directed, only a fraction of the ions impinging on the aluminum plate are sampled by the MS. LTQ calibration mix containing caffeine, MRFA peptide, and Ultramark 1621 was used as the spray solution in all experiments. The dependence of mass spectral intensity on the voltage applied to the different components was tested by scanning the potential of the ellipse from 1 to 6 kV while the sprayer was held at a constant offset of +1 kV in relation to the ellipse potential. The intensities of the protonated caffeine ion (*m/z* 195), MRFA peptide (*m/z* 524), and a peak from the Ultramark 1621 (*m/z* 1322) were recorded as a function of the potential applied to the ellipse.

2.3 Results and Discussion

2.3.1 Focusing of Electrosprayed Ions

A 2D intensity map of ions impinging on the deposition surface was constructed from intensity profiles (dN) at each position along the x-axis, shown in Fig. 2.2. Potentials applied to the sprayer and electrode were 5 and 4 kV, respectively. The resulting intensity plot indicates that the highest ion intensity occurs in the region nearest the spray tip.

Cross-sections (through center of ellipse opening plane, parallel to the y-axis of Fig. 2.2) of spatially resolved ion intensity were recorded using the IonCCD™ while the elliptical electrode was held at a constant potential of 4 kV and the sprayer was positioned 25 mm from the opening plane of the ellipse (z = −25 mm). The spray potential was varied from 4.6 to 6 kV, corresponding to offset potentials of 0.6–2 kV. While an increase in the offset potential increased the overall ion intensity, this also had the effect of broadening the profile (i.e. widening the deposition area). The broadening was likely due to the electrical fields created by the potential difference of the spray tip from the ellipse. The asymmetric nature of the ion beam was most likely the result of the orthogonal position of the sprayer relative to the center axis of the ellipse. The spray was positioned in this manner so that neutral droplets expelled from the spray tip would impinge on the electrode wall rather than be accepted into the MS. The asymmetry is not observed when the

spray direction is in-line with the center axis. The effect the offset voltage (spray potential–ellipse potential) has on both the intensity and spatial distribution of ions exiting the ellipse is shown in Fig. 2.3a.

If one considers the relationship between the maximum recorded intensity as a fraction of the total intensity (I_{max}/I_{tot}) as a function of the potential offset between the spray tip and the focusing potential it is possible to develop a method of quantifying the focal abilities of the electrode under different conditions. A plot of this is shown in Fig. 2.3b. From the plot it is clearly evident that lowering the potential offset of the spray tip from the focusing potential results in greatly increased focal abilities. Additionally, the asymmetric nature of the ion distribution is almost entirely eliminated at lower potentials compared to the distributions obtained at higher offset potentials. While a smaller number of ions are created, the

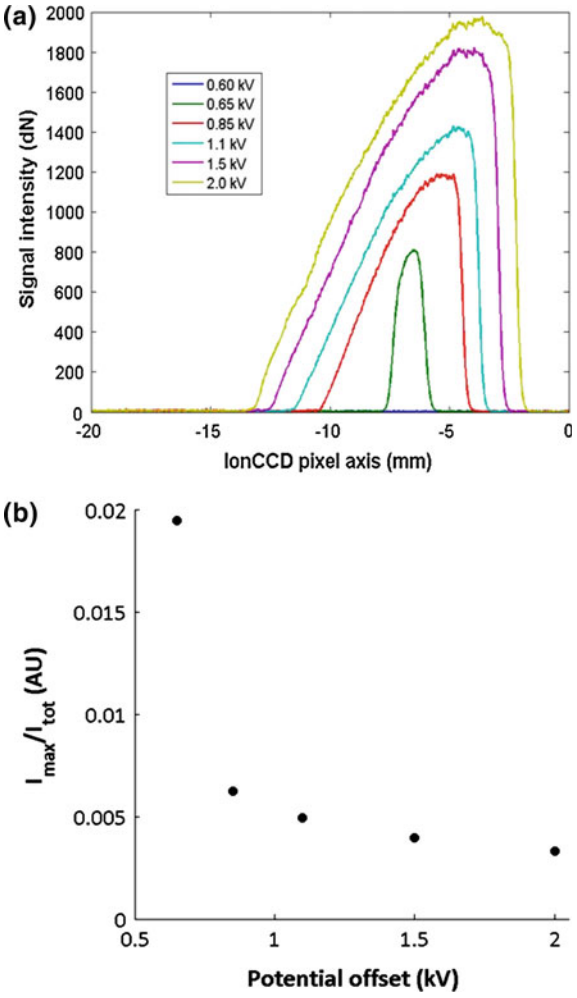

Fig. 2.3 **a** Ion intensity profile at different offset voltages and **b** maximum IonCCD™ signal (I_{max}) as a fraction of total signal (I_{tot}) for different offset potentials. Potential applied to ellipse was 4 kV and sprayer was 25 mm from the ellipse opening plane (z = −25 mm) for values shown. Spray was in the direction of decreasing values on the IonCCD™ pixel axis. The electrode arrangement corresponds to that shown in Fig. 2.1

better focusing will allow a larger percentage of ions to be sampled by a mass spectrometer, improving overall efficiency and reducing the sample volume needed for analysis. This effect is likely due to the repulsive nature of ESI plume, which is magnified at higher potentials as the density of charge increases at the spray tip.

The effect of a gas flow on the focal and transport properties of the device was examined by subjecting the ions to a nitrogen flow from a compressed gas cylinder. The pressure of the nitrogen line, as determined by the regulator, was approximately 5 psi and the interior of the device was assumed to be at atmospheric pressure. Spatial ion distributions were recorded by the IonCCD™ at different offset potentials while the ellipse potential was held constant in the same manner as described earlier. Results of these experiments show an increased intensity and an increased symmetry in the ion beam cross-section; however, the better focus at low offset potentials was not observed. This effect is likely due to the transport of ions and charged microdroplets from areas of low electric field strengths to those of higher strength where they are more highly influenced by electrostatics. Additionally, the removal of solvent vapor decreases its partial pressure within the spray plume to afford more effective solvent evaporation according to Henry's Law.

2.3.2 Simulated Ion Trajectories

A simulated map of the ion flux at the grounded deposition plate is shown in Fig. 2.4. Each of the images in the figure show the predicted effect of altering the potential applied to the spray emitter. From these results it is evident that altering this potential is likely to have a noticeable effect on the resulting ion beam shape as it exits the electrode. A range of different ion mobilities was explored via simulation, each providing the same resulting intensity plots at the grounded plate. It is important to note that these simulations do not attempt to predict the overall intensity difference under these varied conditions. The total ion current is much greater at higher emitter potentials so it is reasonably expected that the true current at the surface would in fact be much greater in Fig. 2.4c when compared with Fig. 2.4a.

While space charge plays a role in determining the trajectories of ions within the electrode, the methods of incorporating space charge included with SIMION do not effectively model the space charge interaction at ion sources. Because of this, these effects were not included in the simulations of ion motion in the elliptical electrode. Instead, ions were given an initial filled sphere distribution centered at different locations relative to the nanoESI spray tip. This method allows for a qualitative understanding of trajectories ions undergo in the elliptical electrode to aid in the improvement of electrode designs.

The simulated contour plots of ion intensity when the spray emitter is set 1 kV above that of the elliptical electrode appear to mimic the shape of the experimentally mapped ion intensity (to a limited extent) as measured with the IonCCD™ detector. As the spray potential is raised (in relation to the focusing potential), this

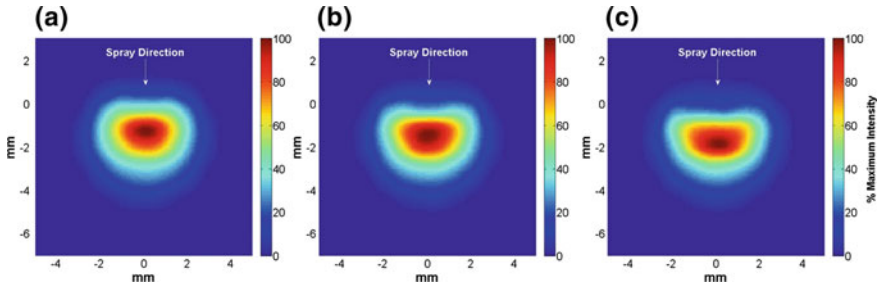

Fig. 2.4 Contour plots of simulated ion intensity at the ground plate of the ellipse for sprayer potentials of **a** 6, **b** 6.5, and **c** 7 kV. Ellipse potential was 5 kV in all cases. Ions were given a filled-sphere initial distribution with radius of 1 cm, centered 0.5 cm below the axis of the ellipse, directly below the spray tip (25 mm from opening plane of ellipse). (0, 0) coordinate corresponds to the center of ellipse opening plane

correlation no longer holds, yet the experimentally observed result of a broadened ion beam is apparent. One likely reason for this disagreement between experiment and simulation is that the phenomenon of charged droplet trajectories from a spray tip is not well modeled with the SIMION-SDS model. The effects of droplet evaporation, droplet breakup, and the differing velocities of droplets ejected from the tip in the range of potentials studied are not considered. The use of the SIMION-SDS algorithm did however, allow for a qualitative study and understanding of ion behavior inside the elliptical electrode.

2.3.3 Ion Transport Efficiency

The overall efficiency of ionization by nanoESI and ion/charged droplet transport to a collector surface was measured with and without using the elliptical focusing electrode through the deposition of the dye rhodamine B. The sprayer was 17 mm from the grounded aluminum collection plate (15 mm from the opening plane of the ellipse) in both experiments while voltages of 4 and 5.5 kV were applied to the ellipse and sprayer (1.5 kV difference) in the experiment with the focusing electrode and a spray potential of 1.5 kV was used without the ellipsoidal lens. Rhodamine B was diluted in 4:1 methanol:water (60 μL, 1 mM) and sprayed at a grounded aluminum plate. Following the deposition, the resulting material on a 1 cm^2 area on the grounded aluminum collection surface, (centered on the deposition area), was redissolved in 1:1 methanol:water (v:v), diluted to a known volume and analyzed for concentration by UV–Vis spectrophotometry. Around 15 % of the rhodamine B in the spray solution was deposited in the 1 cm^2 collection area using nanoESI without the elliptical electrode. With the elliptical electrode and using the same sprayer to counter electrode distance, the entire visible spot was confined within the 1 cm^2 collection area. Measurement of the concentration of the

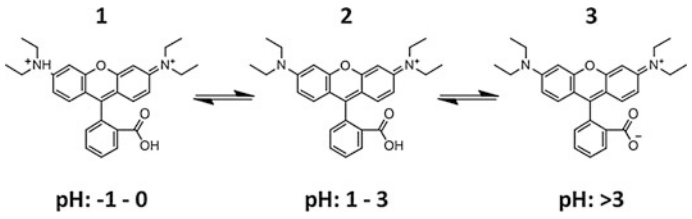

Scheme 2.1 Rhodamine B species in solution at low pH *1*, moderate pH *2*, and high pH *3*

dye taken up in a fixed volume of solvent showed that the contents of this spot corresponded to 70 % of the theoretical yield. These results show that the elliptical electrode is able to concentrate ions/charged droplets into the deposition area to produce a four-fold increase in ion intensity when compared to nanoESI without the use of a focusing electrode. The 1 cm^2 collection area was chosen to represent applications in ambient surface preparation techniques. It is not representative of applications in which ion transfer into a mass spectrometer from an atmospheric pressure ion source is of interest; in such cases the sprayer would be placed closer to a much smaller entrance capillary.

It should be noted that the 70 % efficiency value measured includes both ionization and transport to the collector surface and both processes individually must therefore be highly efficient. Attempts to draw distinctions between dry ion, solvated ion, and charged droplet focusing were not made, as these are all instances of charged particle focusing which was the objective of the experiment; however, it does seem to be important to determine the significance of the transport of analyte in the form of charged droplets. To make this distinction, the above deposition experiments were repeated using a rhodamine B solution doped with ammonium hydroxide, to give a pH of approximately 9 (0.148 M NH_4OH). Rhodamine B exists in three different forms which depend on the solution pH, as shown in Scheme 2.1 [31].

At low pH (−1 to 0) form 1 is favored, but in a solution of moderate pH (1–3), as is found in the spray solution absent a pH modifier, the cation 2 can be assumed. In a solution of higher pH the zwitterion (3) will be the favored form. Although droplet desolvation during drying in air will result in a lowered pH, this is assumed to contribute minor changes to the form of rhodamine B as the change is rarely more than 2 pH units [32]. Because of this it is assumed the deposition at low to moderate pH involves ionic species while at high pH the zwitterion should dominate. The deposition of the basic ammonium solution showed a deposition efficiency of 10 % when compared to theoretical yield (with the use of the elliptical electrode). These results are indicative of the large role played by solution phase ions in the conveyance of chemical species by electrospray, as the zwitterion (3) is effectively neutral, limiting transport to a mechanism associated with charged droplets and incidental neutral collisions.

2.3.4 Mass Spectrometer Interface

The transport of ions from the elliptical lens to the MS was investigated by comparing the ion signal recorded by the MS using the elliptical electrode to the intensities recorded by nanoESI without the electrode but with the same tip to inlet distance. When the elliptical electrode was used potentials of 3 and 4 kV were supplied to the ellipse and sprayer, respectively, while the spray tip was 22 mm from the MS inlet. For the study of intensities without the use of the ellipse, the sprayer was again positioned 22 mm from the inlet and was shielded from air currents that might disrupt the signal intensity. The potential applied to the sprayer in this case was 1 kV to match the offset potential used when the elliptical electrode

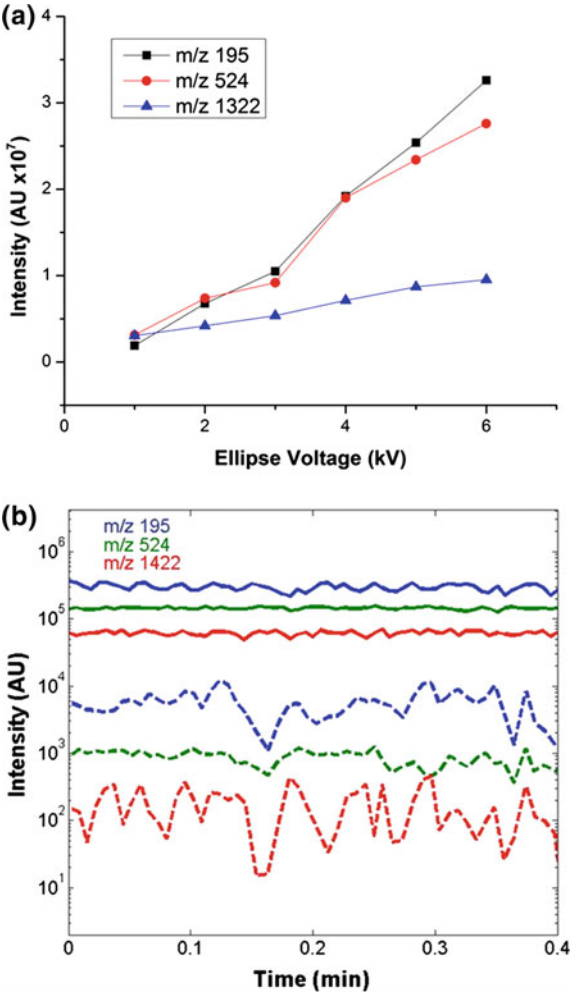

Fig. 2.5 Intensities of different ions detected by MS as a function of potential applied to elliptical electrode: **a** sprayer potential held 1 kV higher than ellipse potential throughout scan and **b** chromatograms of ion intensities using the ellipse electrode (*solid lines*) and without the ellipse electrode (*dashed lines*). Potentials of 3 and 4 kV were applied to the ellipse and sprayer, respectively. For nanoESI without the elliptical electrode, spray potential was 1 kV. In **a** the sprayer was 27 mm from the inlet of the LTQ. Tip to inlet distance for Fig. 2.6b was 22 mm

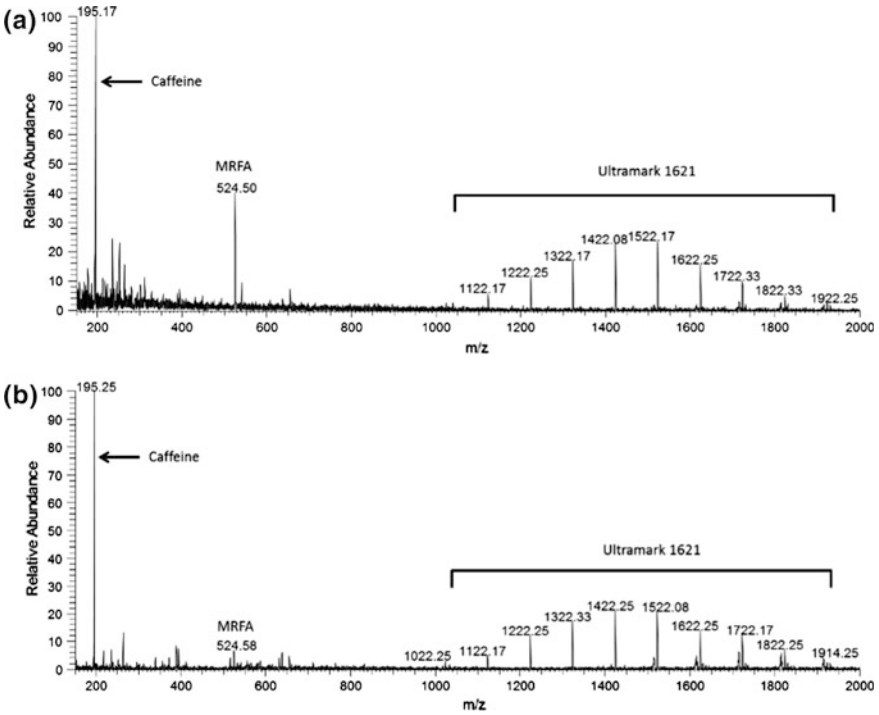

Fig. 2.6 **a** Spectrum recorded for LTQ calibration solution using the elliptical electrode with potentials of 6 and 5 kV applied to the sprayer and ellipse, respectively and **b** spectrum taken for LTQ calibration solution without the use of the focusing electrode at a spray potential of 1 kV. The spray tip to inlet distance was 22 and 3.3 mm in **a** and **b**, respectively

was employed. Figure 2.5b shows the result of these experiments by plotting a chromatogram of several ions characteristic of the calibration solution.

The results shown in Fig. 2.5a clearly indicate that increasing the potential of the electrode and sprayer results in an increased number of ions delivered to the mass spectrometer. With the larger ion (*m/z* 1322), the intensity increase is not as dramatic. As larger ions are less mobile than their smaller counterparts, they are transported to the inlet at a slower rate so that less signal is observed. The result is an increased sensitivity for smaller ions when using the elliptical electrode. Up to an 100 fold enhancement of ion signal was achieved with the use of the elliptical electrode at distances of several centimeters. It must be noted that intensities higher than those obtained with the elliptical electrode are possible through the use of nanoESI alone. This is accomplished by placing the spray tip in close proximity (2–5 mm) to the inlet; however, this does not always allow for sufficient evaporation of solvent and the spectra obtained are remarkably different in regards to relative ion intensity. Additionally, operation in this manner has the potential to introduce a large amount of contamination on the inlet of the mass spectrometer, manifested as carryover between experiments. One exemplary result of the use of the elliptical

electrode was a 4-fold increase in the signal to noise ratio for the detection of MRFA peptide (*m/z* 524) over that achieved even at optimum proximity for nanoESI without the focusing electrode (Fig. 2.6).

The congested appearance of the *m/z* 150–300 range in Fig. 2.6a also supports the conjecture of a mobility dependent ion delivery when using the ellipsoidal electrode as these ions are the same as those seen in low abundance in Fig. 2.6b. A spray distance of several centimeters is impractical for normal nanoESI analysis, but this distance allows for the inclusion of additional sprayers at different distances when the objective of the experiment is to obtain large ion currents. Such cases include ion soft landing, surface modification using ions under ambient conditions, as well as the exploration of novel chemistry observed in ambient ion-molecule reactions in which higher yields remain an issue for practical use.

2.4 Conclusions

In this study simple DC-only potentials were applied to an ellipsoidal focusing element to focus organic ions generated by nanoESI in air. The ion focusing depends on the voltage of the elliptical electrode, that of the ion source, and the distance between the source and the MS aperture. Focusing improved signal in experiments representative of two scenarios: (i) atmospheric pressure surface modification of a relatively large surface area using an ion beams and (ii) ion introduction into a mass spectrometer from a sprayer placed at a fixed and relatively large distance from the inlet. In the first type of experiment an ion transport efficiency of 70 % and a stable signal was achieved relative to ca. 15 % without focusing. In the second type of experiment the relative intensity for the peptide MRFA was four times larger at 22 mm with the focusing lens than it was at 3.3 mm without focusing. Simulations of ion motion matched experiments reasonably well in consideration of the simplified simulation environment employed.

References

1. P. Wang, J. Laskin, Angew. Chem. Int. Ed. **47**, 6678–6680 (2008)
2. D.C. Lim, R. Dietsche, M. Bubek, T. Ketterer, G. Ganteför, Y.D. Kim, Chem. Phys. Lett. **439**, 364–368 (2007)
3. S. Tepavcevic, A.T. Wroble, M. Bissen, D.J. Wallace, Y. Choi, L. Hanley, J. Phys. Chem. B **109**, 7134–7140 (2005)
4. S. Lee, L.M. Molina, M.J. López, J.A. Alonso, B. Hammer, B. Lee, S. Seifert, R.E. Winans, J. W. Elam, M.J. Pellin, S. Vajda, Angew. Chem. Int. Ed. **48**, 1467–1471 (2009)
5. H.J. Rader, A. Rouhanipour, A.M. Talarico, V. Palermo, P. Samori, K. Mullen, Nat. Mater. **5**, 276–280 (2006)
6. N. Thontasen, G. Levita, N. Malinowski, Z. Deng, S. Rauschenbach, K. Kern, J. Phys. Chem. C **114**, 17768–17772 (2010)
7. J. Cyriac, T. Pradeep, H. Kang, R. Souda, R.G. Cooks, Chem. Rev. **112**, 5356–5411 (2012)

8. K.J. Kitching, H.N. Lee, W.T. Elam, E.E. Johnston, H. MacGregor, R.J. Miller, F. Turecek, B.D. Ratner, Rev. Sci. Instrum. **74**, 4832–4839 (2003)
9. M. Volný, W.T. Elam, A. Branca, B.D. Ratner, F. Tureček, Anal. Chem. **77**, 4890–4896 (2005)
10. A. Badu-Tawiah, J. Cyriac, R. Cooks, J. Am. Soc. Mass Spectrom. **23**, 842–849 (2012)
11. A.K. Badu-Tawiah, C. Wu, R.G. Cooks, Anal. Chem. **83**, 2648–2654 (2011)
12. G.E. Johnson, Q. Hu, J. Laskin, Annu. Rev. Anal. Chem. **4**, 83–104 (2011)
13. , US20030157269A1, 2003
14. L. Hanley, S.B. Sinnott, Surf. Sci. **500**, 500–522 (2002)
15. D.R. Ifa, C. Wu, Z. Ouyang, R.G. Cooks, Analyst **135**, 669–681 (2010)
16. S. National Research Council, *Plasma Processing of Materials: Scientific Opportunities and Technological Challenges* 9780309583756 (National Academies Press, Washington, DC, USA, 1991)
17. A.T. Wroble, J. Wildeman, D.J. Asunskis, L. Hanley, Thin Solid Films **516**, 7386–7392 (2008)
18. D.J. Weston, Analyst **135**, 661–668 (2010)
19. M.-Z. Huang, C.-H. Yuan, S.-C. Cheng, Y.-T. Cho, J. Shiea, Annu. Rev. Anal. Chem. **3**, 43–65 (2010)
20. I. Cotte-Rodriguez, R.G. Cooks, Chem. Commun. 2968–2970 (2006)
21. S. Garimella, W. Xu, G. Huang, J.D. Harper, R.G. Cooks, Z. Ouyang, J. Mass Spectrom. **47**, 201–207 (2012)
22. J.S. Page, R.T. Kelly, K. Tang, R.D. Smith, J. Am. Soc. Mass Spectrom. **18**, 1582–1590 (2007)
23. J.B. Fenn, M. Mann, C.K. Meng, S.F. Wong, C.M. Whitehouse, Mass Spectrom. Rev. **9**, 37–70 (1990)
24. P. Kebarle, L. Tang, Anal. Chem. **65**, 972A–986A (1993)
25. N.B. Cech, C.G. Enke, Mass Spectrom. Rev. **20**, 362–387 (2001)
26. D. Douglas, J. French, J. Am. Soc. Mass Spectrom. **3**, 398–408 (1992)
27. A.V. Tolmachev, I.V. Chernushevich, A.F. Dodonov, K.G. Standing, Nucl. Instrum. Methods Phys. Res., Sect. B **124**, 112–119 (1997)
28. R.T. Kelly, A.V. Tolmachev, J.S. Page, K. Tang, R.D. Smith, Mass Spectrom. Rev. **29**, 294–312 (2010)
29. K. Giles, S.D. Pringle, K.R. Worthington, D. Little, J.L. Wildgoose, R.H. Bateman, Rapid Commun. Mass Spectrom. **18**, 2401–2414 (2004)
30. K.J. Gillig, B.T. Ruotolo, E.G. Stone, D.H. Russell, Int. J. Mass Spectrom. **239**, 43–49 (2004)
31. R.W. Ramette, E.B. Sandell, J. Am. Chem. Soc. **78**, 4872–4878 (1956)
32. S. Zhou, B.S. Prebyl, K.D. Cook, Anal. Chem. **74**, 4885–4888 (2002)

http://www.springer.com/978-3-319-49868-3

Manipulation and Characterization of Electrosprayed Ions Under Ambient Conditions
Methods and Instrumentation
Baird, Z.
2017, XVIII, 65 p. 25 illus., 21 illus. in color., Hardcover
ISBN: 978-3-319-49868-3